Puffing/micro-explosion in composite fuel/water droplets heated in flames

D.V. Antonov[1], R.M. Fedorenko[1], P.A. Strizhak[1], Z. Nissar[2], S.S. Sazhin[3*]

[1] *National Research Tomsk Polytechnic University, 30 Lenin Avenue, Tomsk, 634050, Russia*

[2] *Center for Automotive Research and Electric Mobility (CAREM), Universiti Teknologi PETRONAS, 32610 - Seri Iskandar, Perak, Malaysia*

[3] *Advanced Engineering Centre, University of Brighton, Brighton, BN2 4GJ, UK*

June 29, 2021

Abstract

The results of new experimental and theoretical investigations of puffing and micro-explosion of rapeseed oil/water droplets placed in ethanol and propane/butane mixture flames are presented. It is pointed out that time to puffing/micro-explosion increases with increasing initial droplet radii in both flames. This time is always shorter for a propane/butane mixture flame (with maximal temperature 1,450 K) than for an ethanol flame (with maximal temperature 1,120 K). The experimental results are interpreted in terms of a simplified model of the phenomenon, in which it is assumed that a spherical water subdroplet is placed exactly in the centre of a spherical fuel droplet. The start of puffing/micro-explosion is linked with the time instant when the temperature at the water/rapeseed oil interface reaches the water nucleation temperature. The contributions of thermal radiation and supporting wire are taken into account for the first time for the analysis of the phenomena. It is shown that the model predictions agree with experimental data.

Key words:

Micro-explosions, puffing, rapeseed oil, water, ethanol flame, propane/butane

*Corresponding author; e-mail: S.Sazhin@brighton.ac.uk

mixture flame, thermal radiation

1. Introduction

It is well known that heating of composite fuel/water droplets leads to their rapid disintegration due to the difference in nucleation temperatures of water and fuel [1, 2]. These composite droplets could be either two-component, with a clear interface between the fuel and the water subdroplet inside the fuel droplet, or emulsions in which water micro-droplets are almost homogeneously distributed inside a fuel droplet. Droplet disintegration could be local and partial, known as puffing, or complete, known as micro-explosion.

Various engineering and environmental applications of these processes include improvement of the performance of internal combustion engines (see the discussion in [3]) and the extinguishing of fires [4]. This stimulated numerous experimental and theoretical studies of the phenomenon, including its most advanced modelling using Direct Numerical Simulation (DNS)[5, 6, 7] and a relatively simple model described in [8]. At the same time, most of research in this direction was focused on droplets injected into a relatively low temperature gas (below 1000 K) when the effect of thermal radiation on droplet heating could be expected to be relatively small. Among relatively few exceptions are [9, 10]. In [9] a trans-critical evaporation and micro-explosion sub-model for multi-component droplets is suggested. This model was used to investigate micro-explosions of ethanol-Diesel droplets in a Diesel engine-like environment. Spray in these conditions was simulated, ignoring the effects of thermal radiation, and the occurrence of micro-explosions was confirmed. In [10] the results of experimental studies of combustion of a single droplet of fuel suspension, placed into a hot still air at temperatures in the range 700 to 1,000°C, are presented. The conditions (droplet composition and temperature) under which micro-explosions occurred were investigated.

The main aim of the current paper is to investigate puffing/micro-explosion phenomena in ambient gas at temperatures above 1,000 K. We will describe the

results of our investigation of puffing and micro-explosion of two-component and emulsion droplets placed directly in a high temperature (above 1,000 K) flame and describe an approach to the modelling of some features of the phenomena. Relatively large droplets, investigated in our experiments, with initial radii more than about 0.5 mm, have been used in many industrial applications (e.g [11, 12]). Temperature profiles close to those used in our experiments were observed in aero-engine combustion chambers [13] and swirl stabilised combustors [14].

As in [2], the model used in our analysis is based on the analytical solution to the heat conduction equation in a composite droplet, with the Robin boundary condition at its surface, incorporated into a numerical code. Although this solution incorporates the effects of thermal radiation, they were ignored in the analysis presented in [2]. In contrast to [2], they will be taken into account in the present analysis. Moreover, the model described in [2] will be generalised to take into account the contributions of supporting fibres using the approach described in [15].

The experimental set-up is briefly described in Section 2. The experimental results are presented and analysed in Section 3. A description of the model used for the analysis of these results is given in Section 4. The experimental and modelling results are compared in Section 5. In Section 6 the most important results of the paper are summarised.

2. Experimental set-up

Our analysis is focused mainly on composite rapeseed oil/water droplets with volume fractions of rapeseed oil and water taken equal to 90% and 10%, respectively. The methodology of droplet generation used in our analysis is the same as described in [16].

The set-up used in our experiments is schematically presented in Figure 1a. The flames were generated by either an ethanol or propane/butane mixture burner. In the first case, the maximal temperature in the flame was 1,120 K, while in the second case it reached 1,450 K. These temperatures were controlled

by a National Instruments data collection complex and low-inertia thermocouples.

The errors of measurements were estimated as the sums of systematic and random errors. Random errors Δ_r were estimated as:

$$\Delta_r = t(\alpha_c, n)S, \tag{1}$$

where $t(\alpha_c, n)$ is the Student's coefficient, depending on the number of measurements n and confidence level α, assumed equal to 0.95; S is the root squared deviation for a series of measurements.

The total errors in temperature (time) measurements were estimated as ±45 K (±0.1 s). The system was calibrated by measuring temperatures inside the flame at various cross-sections and at various distances from the burner at steps of 0.5 cm or shorter. The scheme and results of temperature measurements are shown in Figure 1b.

The droplets were placed into the registration zone using the coordinate mechanism with a holder (nichrome wires with a diameter of 0.2 mm) at its tip. The width of the flame front in our experiments did not exceed 10 mm which allowed us to minimise the droplet transit time in a variable temperature field. This time did not exceed 5 ms, which was approximately 20-80 times less than typical times to puffing/micro-explosion. Gas temperature in the vicinity of droplets was controlled to ensure that the variations of this temperature due to flame oscillations did not exceed ±45 K. The results of experiments in which the variations of gas temperature exceeded this limit were excluded from our analysis.

The registration zone was illuminated with the help of a MultiLed QT projector (GS Vitec GmbH, Germany) to improve the image contrast of the parent and child droplets. The projector had the following parameters: 15° lens; luminous flux 12,000 Lumen (white); power 150 W. A MultiLed G8 controller was used to measure light intensity (0-100%). The processes of droplet heating, evaporation and break-up were recorded using a slow-motion video camera; a Phantom Miro M310 (Vision Research, USA). The latter had the following

specifications: 3260 frames per second at a resolution of 1280×800 pixels; 12 bit depth; 1 μs minimum exposure; pixel size 20 μm; 12 GB memory; image-based auto-trigger.

In our experiments we used 5400 frames per second at a resolution of 768×768 pixels. The resulting video clips were processed with the help of the Phantom Camera Control software to obtain times to droplet break-up, and parent and child droplet sizes. The sums of the systematic and random errors of estimating these parameters were less than 0.05 s, and 0.025 mm, respectively. The initial droplet radii R_{d0} were measured immediately before their introduction into the flame. Non-sphericity of droplets was accounted for by averaging the droplet sizes obtained for two perpendicular cross-sections

The efficiency of droplet break-up can be estimated as the ratio of the total areas of the child droplets (S_c) to the area of the parent droplet (S_0). Assuming that the radii of child droplets are the same (r_c) and keeping in mind that in the absence of evaporation the total volume of parent and child droplets are the same, it can be shown that $S_c/S_0 = R_{d0}/r_c$. We appreciate the crudeness of this assumption, but we had to use it to estimate the total surface area of droplets including those outside the focus of our camera. The actual distributions of droplets by sizes will be illustrated at the end of Section 4.

The details of our approach to estimation of the number and average radii of child droplets are given in Appendix 1.

The processing of video clips included not only the binarisation of images, but also the determination of the lens depth of field. This made it possible to estimate the number of droplets both in the lens depth of field and outside this depth. To take into account the contribution of child droplets outside this depth additional experiments were performed in which this depth varied. The corresponding correction coefficients for determination of the numbers and sizes of the droplets were obtained.

The depth of field of the Nikon lens (200 mm f/4 AF-D Macro) was calculated as $P = R_1 - R_2$, where R_1 and R_2 are the front and back boundaries of the depth of field. The DOF 5-15 Depth of Field Target was used for determination of the

depth of focus. DOF 5-15 includes two sets of scales. When viewed at an angle of 45° each scale consists of horizontal and vertical lines with densities of 5 and 15 pairs per mm, respectively. This special calibration target was designed to estimate the depth of focus without theoretical calculations. In our experiments the depth of focus was in the range 6.5 mm to 9 mm for diafragm numbers in the range 11 to 16. Correction factors for each series of experiments were determined separately. In all experiments manual focusing, using the above-mentioned target, was performed. This allowed us to estimate the depth of field of the lens by placing the target in the registration zone. Then the target was focused manually and the distance over which it was still in focus was measured directly. Thus the lens depth was determined.

The same procedure was used for determining the scale factor in mm/pixel. At least 3 pixels were used for the smallest child droplets. The registration areas were in the range 10×10 mm to 15×15 mm.

Note that the arrangement for droplet heating used in our analysis is different from the one used in our previous studies (e.g. [17]). We performed the experiments at much higher temperatures than those used in [17] (up to 1450 K), which allowed us to investigate for the first time, to the best of our knowledge, the effects of thermal radiation on droplet puffing/micro-explosion.

3. Experimental results

As follows from the analysis of video frames, for droplets placed in the ethanol flame with ambient gas temperatures below 1000 K the fragmentation of emulsion droplets takes place via puffing, while for gas temperatures in the range 1055 to 1120 K, 60-70% disintegrated via micro-explosions while 30-40% of droplets disintegrated via puffing. In all cases, the disintegration of two-component droplets took place via puffing leading to micro-explosions, or directly via micro-explosion. 5-10 experiments were performed for each of six temperatures in the range 880 to 1120 K. Some examples of our observations are illustrated in Figure 2. Similar footages were obtained from the experiments

with the propane/butane mixture flame.

Video clips showing the examples of the dynamics of puffing and micro-explosion of droplets in our experiments are presented in Supplementary Material A (Emulsion droplet, $R_{d0} = 0.778 \pm 0.025$ mm, $T_g = 1064 \pm 45$ K), Supplementary Material B (Emulsion droplet, $R_{d0} = 0.787 \pm 0.025$ mm, $T_g = 920 \pm 45$ K) and Supplementary Material C (Composite droplet, $R_{d0} = 0.787 \pm 0.025$ mm, $T_g = 920 \pm 45$ K). In all cases, rapeseed and water contents were 90% and 10%, respectively.

The plots of time to puffing/micro-explosion (τ_p) of two-component droplets, introduced into ethanol and propane/butane mixture flames, versus their initial radii R_{d0}, are presented in Figure 3. As follows from this figure, for both flames τ_p increases when R_{d0} increases in agreement with the previously obtained results for lower ambient gas temperatures [1, 3]. For all R_{d0}, the values of τ_p were always shorter for droplets in the propane/butane mixture flame than for those in the ethanol flame. This is attributed to higher gas temperatures in the propane/butane mixture flame compared with those in the ethanol flame (see Figure 1b).

As in the case of gas temperature measurements (see Figure 1b), the error bars shown in Figure 3 and the following figures are the sums of systematic and random errors. Random errors were estimated based on Formula (1). Large error bars are attributed to the effects of several factors on the processes under consideration. Perhaps the most important of these factors is the uncertainty of the initial location of the water subdroplet inside the water droplet and the change in its location during the heating period.

The plots of time to puffing (micro-explosion) (τ_p) in two-component and emulsion droplets versus ambient gas temperature in the ethanol flame are shown in Figure 4a. The experiments were performed for the range of heights above the base 0.5 cm to 3.5 cm. As can be seen from this figure, τ_p decreases with increasing ambient gas temperature for both types of droplets in agreement with our earlier results [1]. In all cases, τ_p for emulsion droplets was shorter than that for two-component droplets. The plots of τ_p versus height h for the

same droplets and flames are shown in Figure 4b. It follows from this figure that minimal values of τ_p were observed at h close to 2 cm. This location is close to where the maximal gas temperature was observed (see Figure 1b).

Ratios of the total mean surface areas of emulsion and two-component droplets after (when child droplets were formed) and before their disintegration (S_c/S_0) versus ambient gas temperatures are shown in Figure 5. Droplet initial parameters are the same as in Figure 4. As can be seen in Figure 5, S_c/S_0 for two-component droplets is always larger than that for emulsion droplets. This is related to the fact that the two-component droplets were disintegrated via micro-explosions. Micro-explosions dominated for the emulsion droplets at temperatures above 1000 K (about 60%-70% of cases), but below this temperature these droplets disintegrated via puffing. Much smaller droplets were produced during micro-explosion than during puffing. For both types of droplet S_c/S_0 increases when ambient temperature increases. This shows that at higher temperatures both puffing and micro-explosion processes intensify leading to generation of smaller child droplets.

Note that the results shown in Figure 5 were based on a rather crude assumption that all child droplets are the same size (see Section 2). Actual distributions of child droplets by radii after puffing and micro-explosion events for gas temperature equal to 1120 K are shown in Figure 6. As follows from this figure, puffing leads to generation of larger droplets than does micro-explosion. When the number of child droplets generated during micro-explosion was at its peak, their radii were 0.025 mm, while when the number of child droplets generated during puffing was at its peak, their radii were 0.035 mm.

4. Modelling of the phenomena

The analysis of the experimental results presented in the previous section is based on the model described in [2]. The main assumption of this model, when applied to our data, is that a spherical water subdroplet of radius R_w is located in the centre of a rapeseed oil droplet of radius R_d. The time evolution of tem-

perature T in this composite droplet was described in terms of the 1D transient heat conduction equation. The analytical solution to this equation, based on the Robin boundary condition at the surface of the rapeseed oil (fuel) droplet and continuity conditions at the rapeseed oil/water interface, was obtained in the form:

$$T = \frac{1}{R_d \xi}\left[\sum_{n=1}^{\infty} \Theta_n(t) v_n(\xi) + \frac{\mu_0 \xi}{1+h_0}\right], \tag{2}$$

where

$$\Theta_n(t) = (q_n + f_n \mu_0) \exp\left(-\frac{\lambda_n^2 t}{R_d^2}\right) + \frac{p_n}{\lambda_n^2}\left[1 - \exp\left(-\frac{\lambda_n^2 t}{R_d^2}\right)\right],$$

$$f_n = \frac{1}{||v_n||^2}\int_0^1 f(\xi) v_n(\xi) b \mathrm{d}\xi$$

$$= \frac{1}{||v_n||^2}\left\{\int_0^{\xi_w} \frac{-\xi}{1+h_0}\frac{\sin(\lambda_n a_w \xi)}{\sin(\lambda_n a_w \xi_w)} k_w a_w^2 \mathrm{d}\xi + \int_{\xi_w}^1 \frac{-\xi}{1+h_0}\frac{\sin(\lambda_n a_f \xi + \beta_n)}{\sin(\lambda_n a_f \xi_w + \beta_n)} k_f a_f^2 \mathrm{d}\xi\right\}$$

$$q_n = \frac{1}{||v_n||^2}\int_0^1 F_0(\xi) v_n(\xi) b \mathrm{d}\xi$$

$$= \frac{1}{||v_n||^2}\left\{\int_0^{\xi_w} R_d \xi T_0(R_d\xi)\frac{\sin(\lambda_n a_w \xi)}{\sin(\lambda_n a_w \xi_w)} k_w a_w^2 \mathrm{d}\xi + \int_{\xi_w}^1 R_d \xi T_0(R_d\xi)\frac{\sin(\lambda_n a_f \xi + \beta_n)}{\sin(\lambda_n a_f \xi_w + \beta_n)} k_f a_f^2 \mathrm{d}\xi\right\}$$

$$p_n = \frac{1}{||v_n||^2}\int_0^1 R_d^3 \xi \tilde{P}(\xi) v_n(\xi) b \mathrm{d}\xi$$

$$= \frac{1}{||v_n||^2}\left\{\int_0^{\xi_w} R_d^3 \xi \tilde{P}(\xi)\frac{\sin(\lambda_n a_w \xi)}{\sin(\lambda_n a_w \xi_w)} k_w a_w^2 \mathrm{d}\xi + \int_{\xi_w}^1 R_d^3 \xi \tilde{P}(\xi)\frac{\sin(\lambda_n a_f \xi + \beta_n)}{\sin(\lambda_n a_f \xi_w + \beta_n)} k_f a_f^2 \mathrm{d}\xi\right\}$$

$$f(\xi) \equiv \frac{-\xi}{1+h_0} = \sum_{n=1}^{\infty} f_n(t) v_n(\xi),$$

$$F_0(\xi) \equiv R_d \xi T_0(R_d\xi) = \sum_{n=1}^{\infty} q_n(t) v_n(\xi), \quad R_d^3 \xi \tilde{P}(\xi) = \sum_{n=1}^{\infty} p_n(t) v_n(\xi),$$

$$v_n(\xi) = \begin{cases} \frac{\sin(\lambda_n a_w \xi)}{\sin(\lambda_n a_w \xi_w)} & \text{when} \quad 0 \le \xi \le \xi_w \\ \frac{\sin(\lambda_n a_f \xi + \beta_n)}{\sin(\lambda_n a_f \xi_w + \beta_n)} & \text{when} \quad \xi_w < \xi \le 1, \end{cases}$$

β_n is $\beta(\lambda = \lambda_n)$,

$$||v_n||^2 = \int_0^1 v_n^2 b \mathrm{d}\xi = \frac{\sqrt{c_w \rho_w k_w}}{\lambda_n \sin^2(\lambda_n a_w \xi_w)}\left[\frac{a_w \lambda_n \xi_w}{2} - \frac{\sin(2 a_w \lambda_n \xi_w)}{4}\right]$$

$$+\frac{\sqrt{c_f\rho_f k_f}}{\lambda_n \sin^2(\lambda_n a_f \xi_w + \beta_n)}\left\{\frac{a_f\lambda_n(1-\xi_w)}{2} - \frac{\sin(2\lambda_n a_f + 2\beta_n) - \sin(2\lambda_n a_f \xi_w + 2\beta_n)}{4}\right\},$$

$$\beta = \cot^{-1}\left[\frac{k_f - k_w}{k_f a_f \xi_w \lambda} + \frac{k_w a_w}{k_f a_f}\cot\left(a_w\lambda\xi_w\right)\right] + i\pi - a_f\lambda\xi_w,$$

$i = 0, 1, 2, 3, ...$; our analysis was focused on $i = 0$ (the values of v_n are the same for all other values of i).

The equation for a countable set of positive eigenvalues λ_n follows from the boundary condition at $\xi = 1$:

$$\lambda_n a_f \cos(\lambda_n a_f + \beta) + h_0 \sin(\lambda_n a_f + \beta) = 0. \tag{3}$$

These are the parameters used in (2) and (3):

$$H = \frac{h}{k_f} - \frac{1}{R_d}, \quad \mu = \frac{R_d}{k_f}\left(hT_g + \rho_l L_f \dot{R}_d\right), \quad \xi = R/R_d, \quad \tilde{P}(\xi) = P(\xi R_d) = P(R),$$

$$F(t,\xi) = u(t,R) \equiv T(R,t)R, \quad h_0 = HR_d = \frac{hR_d}{k_f} - 1,$$

$$\mu_0 = \mu R_d = \frac{R_d^2}{k_f}\left(hT_g + \rho_l L_f \dot{R}_d\right) = \frac{R_d^2 h T_{\text{eff}}}{k_f}.$$

$$b = \begin{cases} c_w\rho_w & \text{when} \quad 0 \le \xi \le \xi_w \\ c_f\rho_f & \text{when} \quad \xi_w < \xi \le 1 \end{cases},$$

h is the convection heat transfer coefficient; $k_{w(f)}$, $c_{w(f)}$ and $\rho_{w(f)}$ are thermal conductivity, specific heat capacity and density of water (liquid fuel), respectively; R is the distance from the droplet centre ($R \le R_d$). The effects of swelling were considered (see [2] for the details),

$$T_{\text{eff}} = T_g + \frac{\rho_l L \dot{R}_{d(e)}}{h}.$$

The term $\dot{R}_{d(e)} = dR_d/dt$ describes the effect of evaporation; it was calculated using the model suggested by Abramzon and Sirignano [20].

Solution (2) uses the assumption that droplet radius is fixed. This assumption is valid for short time steps during which this solution is used in the numerical code. The changes in droplet radii and other parameters with time are taken into account at the next time step.

The time to puffing/micro-explosion was associated with the time instant when the temperature at the water/rapeseed oil interface became equal to the water nucleation temperature.

The model described above was generalised in a non-self-consistent way to consider the effect of the relative gas-droplet velocity [19] (cf. the application of this model in [21]). This generalisation, however, will not be used in our analysis since this velocity in our experiments was small.

The source term $P(R)$ used in Solution (2) is proportional to the external power density absorbed at a certain point inside the droplet. The contribution of this term was considered in the derivation of (2) but was not investigated in our previous studies [2, 19]. This will be done in the current paper.

Assuming that this power density is provided by external thermal radiation and that radiation is instantaneously and homogeneously absorbed inside the droplet (the validity of this assumption for internal combustion engine conditions was demonstrated in [22]) the dependence of P on R can be ignored and $P(R)$ can be presented as:

$$P(R) \equiv P_r = 3\sigma \bar{Q}_a \theta_R^4 / (R_d c_l \rho_l) \ , \tag{4}$$

where θ_R is the radiative temperature (equal to gas temperature when gas is optically thick and external temperature when gas is optically thin); σ is the Stefan-Boltzmann constant; subscript $_l$ refers to liquid; $\bar{Q}_a$ is the efficiency factor of absorption.

Expression (4) was originally derived for homogeneous droplets. Recalling, however, that the volume fraction of rapeseed oil in our experiments was 90%, for a crude estimate of the effect of thermal radiation we will assume that radiation absorption in composite droplets is the same as in rapeseed oil droplets.

The approximation of $\bar{Q}_a$ for Diesel droplets in the range of radii 5 μm to 200 μm is described in [23]. In our experiments the droplets were much larger than those described in [23] and we cannot use the approximations suggested in that paper. Our estimate of the value of $\bar{Q}_a$ is based on the expression suggested

in [24]:

$$\bar{Q}_a = 1 + \frac{\exp(-2\tau_i)}{\tau_i} - \frac{1 - \exp(-2\tau_i)}{2\tau_i^2}, \tag{5}$$

where $\tau_i = 2\kappa_\lambda x_{d\lambda}$ is the optical thickness of the droplet, $\kappa_\lambda = k_\lambda\lambda/(4\pi)$ and $x_{d\lambda} = 2\pi R_{d0}/\lambda$ are the index of absorption and diffraction parameter of the droplets, respectively; k_λ and λ are the absorption coefficient and wavelength, respectively. Remembering the definitions of κ_λ and $x_{d\lambda}$ we can present the expression for the optical thickness as $\tau_i = k_\lambda R_{d0}$.

As follows from the experimental results presented in [23], for typical Diesel and gasoline fuels $\kappa_\lambda \geq 10^{-3}$. We can assume that the values of the index of absorption for rapeseed oil are comparable with these values. For typical initial radii of the droplets used in our experiments, $R_{d0} = 0.7$ mm, and recalling that the maximal spectral emission power for temperatures in the range between 1000 K to 2000 K (flames used in our experiments) is achieved at $\lambda \approx 2$ μm [25], we obtain $x_{d\lambda} = 2.2 \times 10^3$. Hence, $\tau_i \geq 4.4$. Having substituted this value of τ_i into (5) we obtain the following estimate of the values of $\bar{Q}_a$:

$$0.97 \leq \bar{Q}_a \leq 1. \tag{6}$$

This estimate of $\bar{Q}_a$ allows us to assume that $\bar{Q}_a \approx 1$ in our analysis of the effect of thermal radiation on the initiation of puffing and micro-explosion. This assumption is different from the approximation of droplets by black spheres, for which $\bar{Q}_a = 1$ but all radiation is absorbed at the surface of the droplets, that is commonly used in simplified models for radiation absorption in droplets (see [18] for the discussion of the physical inconsistency of this assumption). Note the mistake in Expression (3.94) of [18].

In our previous papers [2, 19], the effect of a holder supporting the droplet on droplet heating and evaporation was ignored. In our present analysis it is taken into account using the model described in [15]. The latter model makes the assumption that heat supplied to the droplet through the holder is instantaneously distributed throughout the whole volume of the droplet. This allows us to describe the effect of the holder on droplet heating in the same way as we

described the effect of thermal radiation on droplet heating. This is done by introducing the following function to Equation (2)

$$P(R) = P_h \equiv \frac{3k_f(T_{\rm sup} - T_c)}{4\pi c_f \rho_f R_d^4} S_C, \tag{7}$$

where S_C is the contact area between the droplet and holder, estimated as:

$$S_C = \pi d_{\rm h} R_d, \tag{8}$$

$d_{\rm h}$ is the outer diameter of the holder (wire).

The validity of the assumption that heat supplied via the support is homogeneously distributed over the whole volume of droplet follows from our assumption that the effect of this heat is equivalent to internal heating of droplets by thermal radiation and the results of the analysis presented in [22], where it was shown that the effect of the distributed absorption of thermal radiation inside droplets can be replaced by the effect of its homegeneous absorption there.

As in the case of the radiative heating model discussed earlier in this section, when deriving Expression (7) it was assumed that the contribution of water in the droplet to this process can be ignored.

For practical application of Expression (7) one needs to assess the values of $T_{\rm sup}$. In the original application of the model the results of direct measurements of $T_{\rm sup}$ were used assuming that the presence of droplets does not affect $T_{\rm sup}$. Unfortunately, this approach is not applicable to our experimental set-up where flame temperatures are high, as it can lead to unphysical values of $T_{\rm sup}$ above the rapeseed oil boiling temperature. In our analysis we assume that $T_{\rm sup}$ is equal to the surface temperature of the droplet. This assumption is compatible with the basic assumption of the model that there is no temperature gradient along the surface of the droplet, which enabled us to use the one-dimensional model.

The effects of thermal radiation and support are additive. The combined contribution of thermal radiation and the holder to droplet heating is described by the following expression:

$$P(R) = P_r + P_h. \tag{9}$$

Note that the model described in this section is based on the assumption that droplets are spherical. Assuming that one-component non-spherical droplets can be approximated by spheroids, the authors of [26] showed that the effect of their eccentricities on the evaporation time can be considered small for eccentricity values not exceeding 1.5. We anticipate that this result can be extended to the composite droplets considered in our paper, which allows us to apply the model described in this section to droplets which are not strictly spherical.

5. Experimental versus modelling results

A comparison between experimentally observed and predicted times to puffing/micro-explosion (τ_p) for droplets placed in the ethanol and propane/butane mixture flames is presented in Figure 7. The volume fractions of rapeseed oil and water were 90% and 10% respectively. Droplets were located at h= 1.5 ± 0.1 cm where ambient gas temperatures were 1,120 K and 1,400 K for ethanol and propane/butane mixture flames, respectively. Since the measurements took place inside the flames, where gas is optically thick, we assumed that $\theta_R = T_g$. As follows from Figure 7, the effect of the support is relatively small, while the effect of thermal radiation leads to a dramatic reduction in the values of τ_p for both flames. When the effects of both radiation and support are considered, the agreement between the model predictions and experimental data turns out to be very good. In agreement with our previous results both modelling and experimental data show an increase in τ_p with increasing R_{d0}.

Note that the effect of thermal radiation demonstrated in Figure 7 is the maximal possible one as the model used in our analysis is based on the assumption that $\bar{Q}_a = 1$. Realistic values of $\bar{Q}_a$ are expected to be a little smaller than 1 (in the range 0.97 to 1, see Section 4). Note that the effects of thermal radiation for large droplets used in our analysis are much stronger than these for smaller droplets for which $\bar{Q}_a$ are expected to be much smaller than 1. For example, for Diesel fuel droplets with radii close to 10 μn, typical for Diesel engine-like conditions, $\bar{Q}_a$ is close to 0.1 [23].

In all cases presented in Figure 7 the predicted values of τ_p are larger than those observed experimentally. This can be attributed to the key assumption of the model that the water subdroplet is located exactly in the centre of the rapeseed oil droplet. Taking into account any shifting of the water subdroplet from the centre of the rapeseed oil droplet would lead to a reduction in τ_p. The analysis of this effect, however, is outside the scope of this paper.

The times to puffing/micro-explosion of the same droplets as in Figure 7 predicted by the models, based on the assumptions that these processes start when the temperature at the water/rapeseed oil interface (T_w) reaches the water boiling (T_B) and nucleation (T_N) temperatures, are shown in Figure 8. The curves for the latter case are the same as shown in Figure 7. As can be seen in Figure 8, the times to puffing/micro-explosion predicted by the model based on the assumption that puffing/micro-explosion starts when $T_w = T_B$ are shorter than those predicted by the model based on the assumption that this process starts when $T_w = T_N$, as expected. The difference between these times, however, is relatively small and can be ignored in crude estimations of this time.

The results presented in Figures 7 and 8 were obtained by performing calculations in parallel using Matlab R2020a and Wolfram Mathematica v 12.1. The results using the two approaches coincided within the accuracy of plotting. The details of both numerical procedures are described in [2].

6. Conclusions

The results of experimental investigation of the puffing and micro-explosion of rapeseed oil/water droplets placed in ethanol and propane/butane mixture flames are presented. The volume fractions of rapeseed oil and water in the experiments were taken equal to 90% and 10%, respectively. It is pointed out that time to puffing/micro-explosion increased with increasing initial droplet radii in both flames. This time was always shorter for the propane/butane mixture flame (with maximal temperature 1,450 K) than for the ethanol flame (with maximal temperature 1,120 K). The model used for the analysis of exper-

imental data is based on the previously obtained analytical solution to the heat conduction equation for a composite droplet with the Robin boundary condition at its surface. As in the previously developed model of the phenomena [2], a spherical water subdroplet is assumed to be located exactly in the centre of a spherical rapeseed oil droplet. The start of puffing/micro-explosion was associated with the time instant when the temperature of the water/rapeseed oil interface reached the water nucleation temperature. In contrast to the model described in [2] the droplet heating due to absorption of the thermal radiation inside the droplet was taken into account assuming that this radiation leads to homogeneous heating of the droplet. Heating of the droplet via the supporting wire was taken into account using a simplified model in which this heating was assumed to be instantaneously distributed throughout the whole volume of the droplet.

The effect of the supporting wire on time to puffing/micro-explosion is shown to be small, while that of thermal radiation reduced this time by more than 50%. A comparison between the prediction of the model and its simplified version, based on the assumption that the start of puffing/micro-explosion is associated with the time instant when the temperature of the water/rapeseed oil interface reaches the water boiling temperature, showed that the times predicted by the simplified model are less than those predicted by the model used in our analysis by not more than 14%. This reduction can be ignored in many practical applications of the model. The predictions of the model considering the effects of thermal radiation and the droplet support are shown to agree well with experimental data.

Acknowledgements

The work on this paper was supported by National Research Tomsk Polytechnic University (project VIU-ISHFVP-60/2019) (contribution by P.A. Strizhak), Scholarships from the President of the Russian Federation (grants nos. SP-447.2021.1 and MN-7/2260) (contributions by D.V. Antonov and R.M. Fe-

dorenko), the Centre for Automotive Research and Electric Mobility (CAREM) of the Universiti Teknologi PETRONAS (UTP) (supported by the Ministry of Higher Education Fundamental Research Grant Scheme (FRGS) (Grant FRGS/1/2017/TK10/UTP/01/2) and UTP Graduate Assistantship (GA) scheme) (contribution by Z. Nissar) and the Royal Society (UK) (Grant no. IEC 192007) (contribution by S.S. Sazhin).

Appendix

The Shadow Photography method for estimating the number/sizes of child droplets

The Shadow Photography (SP) method was designed for the analysis of shadow images. Three approaches were used to estimate the number density (N_{cd}) and radii (r_{cd}) of child droplets using this method. This allowed us to improve the accuracy and assess the reproducibility of the results. The difference between the results obtained using these approaches did not exceed 5%, which demonstrated the applicability of all these approaches. The first approach was based on the application of the original numerical code in Mathematica [28]. On the video frames obtained during the experiments the time instants when parent droplets disintegrated into child droplets were identified. The images at these time instants were converted into tiff-images and uploaded to Mathematica. The program for the analysis of these images had two parts: 1) identification of the binarisation threshold; 2) the main analyser (identification of the elements, calculation of their number and sizes using the scale coefficient). The background noise was removed in both parts. The work of the main analyser (Morphological Binarizer and Median filter) was to identify contrast images (child droplets) against a light background. All bounded objects were presented as spherical droplets of limited sizes. This was followed by calculation of the number of liquid objects and estimation of the radii of the identified child droplets.

The second approach used for the analysis of images during droplet disinte-

gration was based on the realisation of the SP method in Actual Flow software [27]. In this algorithm, video frames illustrating the formation process of child droplets were selected. Then the images were processed using the following steps. Firstly, low frequency filtration was used to reduce the level of noise. Then the images were binarised using the high frequency Laplace filter. The final step focused on the search for simply connected regions based on binarised images. As a result, an irregular data field containing the coordinates of droplet centres and droplet radii was created for each image. Also, images formed by glare from droplets were removed during this step.

A code developed in Matlab was used in the third approach. This code allowed us not only to determine the number of child droplets and their radii but also a number of other parameters, including maximal, minimal and average radii of child droplets, maximal, minimal and average velocities of these droplets, and their maximal, minimal and average kinetic energies, and surface areas after and before their disintegration. The original video frames obtained during experiments showed time instants when parent droplets disintegrated forming child droplets. Two consecutive video frames showing the puffing/micro-explosion processes were selected, transferred into tiff-images and uploaded to Matlab. During the processing of these images the search for simply connected regions based on binarised images was performed. As a result, an irregular data field containing the coordinates of droplet centres and droplet radii was created as in the case of the second approach. Then a rectangular region, in which child droplets were registered, was selected. Within this region, the search for child droplets was performed. An example of image processing using Matlab is shown in Figure A.

References

[1] D.V. Antonov, G.V. Kuznetsov, P.A. Strizhak, O. Rybdylova, S.S. Sazhin, Micro-explosion and autoignition of compos-

ite fuel/water droplets, Combust. Flame 210 (2019) 479-489. https://doi.org/10.1016/j.combustflame.2019.09.004.

[2] S.S. Sazhin, T. Bar-Kohany, Z. Nissar, D. Antonov, P.A. Strizhak, O.D. Rybdylova, A new approach to modelling micro-explosions in composite droplets. Int. J. Heat Mass Transf. 161 (2020) 120238. https://doi.org/10.1016/j.ijheatmasstransfer.2020.120238.

[3] S.S. Sazhin, O. Rybdylova, C. Crua, M. Heikal, M.A. Ismael, Z. Nissar, A.R.B.A. Aziz, A simple model for puffing/micro-explosions in water-fuel emulsion droplets, Int. J. Heat Mass Transf. 131 (2019) 815-821. https://doi.org/10.1016/j.ijheatmasstransfer.2018.11.065.

[4] G. V. Kuznetsov, M. V. Piskunov, P.A. Strizhak, How to improve efficiency of using water when extinguishing fires through the explosive breakup of drops in a flame: Laboratory and field tests, Int. J. Therm. Sci. 121 (2017) 398-409. https://doi.org/10.1016/j.ijthermalsci.2017.08.004.

[5] S. Fostiropoulos, G. Strotos, N. Nikolopoulos, M. Gavaises, Numerical investigation of heavy fuel oil droplet breakup enhancement with water emulsions, Fuel 278 (2020) 118381. https://doi.org/10.1016/j.fuel.2020.118381.

[6] J. Shinjo, J. Xia, L.C. Ganippa, A. Megaritis, Physics of puffing and microexplosion of emulsion fuel droplets. Phys. Fluids 25 (2014) 103302. https://doi.org/10.1063/1.4897918.

[7] J. Shinjo, J. Xia, A. Megaritis, L.C. Ganippa, R.F. Cracknell, Modeling temperature distribution inside an emulsion fuel droplet under convective heating: A key to predicting microexplosion and puffing, Atomization Sprays 26 (2016) 551-583. https://doi.org/ 10.1615/AtomizSpr.2015013302.

[8] O.G. Girin, Dynamics of the emulsified fuel droplet micro-explosion, Atomization Sprays 27 (2017) 407-422 . https://doi.org/10.1615/AtomizSpr.2017017143.

[9] P. Yi, T. Li, Y. Fu, S. Xie, Transcritical evaporation and microexplosion of ethanol-diesel droplets under diesel engine-like conditions, Fuel 284 (2021) 118892. https://doi.org/10.1016/j.fuel.2020.118892.

[10] D.O. Glushkov, D.V. Feoktistov, G.V. Kuznetsov, K.A. Batishcheva, T. Kudelova, K.K. Paushkina, Conditions and characteristics of droplets breakup for industrial waste-derived fuel suspensions ignited in high-temperature air, Fuel 265 (2020) 116915. https://doi.org/10.1016/j.fuel.2019.116915.

[11] A.A. Boateng, Rotary Kilns: Transport Phenomena and Transport Processes: Second Edition, 2015. Butterworth-Heinemann Inc (Verlag), Elsevier. https://doi.org/10.1016/C2014-0-01966-1.

[12] P.J. Mullinger, N.A. Chigier, The design and performance of internal mixing multijet twin fluid atomizers. J. Inst. Fuel 47 (1974) 251-261.

[13] A.A.A. Gamil, T. Nikolaidis, I. Lelaj, P. Laskaridis, Assessment of numerical radiation models on the heat transfer of an aero-engine combustion chamber. Case Stud. Therm. Eng. 22 (2020) 100772. https://doi.org/10.1016/j.csite.2020.100772.

[14] A.K. Sharma, C. Bhattacharya, S. Sen, A. Mukhopadhyay, A. Datta, Analysis of different radiation models in a swirl stabilized combustor. in ASME 2014 Gas Turbine India Conference, GTINDIA 2014 (2014). https://doi.org/10.1115/GTINDIA2014-8318

[15] P.A. Strizhak, R.S. Volkov, G. Castanet, F. Lemoine, O. Rybdylova, S.S. Sazhin, Heating and evaporation of suspended water droplets: experimental studies and modelling, Int. J. Heat Mass Transf. 127 (2018) 92-106. https://doi.org/10.1016/j.ijheatmasstransfer.2018.06.103.

[16] D. V. Antonov, G. V. Kuznetsov, P.A. Strizhak, Comparison of the characteristics of micro-explosion and ignition of two-fluid water-based droplets, emulsions and suspensions, moving in the high-

temperature oxidizer medium, Acta Astronaut. 160 (2019) 258-269. https://doi.org/10.1016/j.actaastro.2019.04.048.

[17] D. Antonov, M. Piskunov, P. Strizhak, D. Tarlet, J. Bellettre, Dispersed phase structure and micro-explosion behavior under different schemes of water-fuel droplets heating, Fuel 259 (2020) 116241. https://doi.org/10.1016/j.fuel.2019.116241.

[18] S.S. Sazhin, Droplets and Sprays, Springer, 2014.

[19] D.V. Antonov, P.A. Strizhak, R.M. Fedorenko, Z. Nissar, S.S. Sazhin, Puffing and micro-explosions in rapeseed oil/water droplets: the effects of coal micro-particles in water, Fuel 289 (2021) 119814. https://doi.org/10.1016/j.fuel.2020.119814.

[20] B. Abramzon, W.A. Sirignano, Droplet vaporization model for spray combustion calculations, Int. J. Heat Mass Transf. 32 (9) (1989) 1605-1618. https://doi.org/10.1016/0017-9310(89)90043-4.

[21] D.V. Antonov, R.M. Fedorenko, P.A. Strizhak, G. Castanet, S.S. Sazhin, Puffing/micro-explosion of two closely spaced composite droplets in tandem: experimental results and modelling, Int. J. Heat Mass Transf. 176 (2021) 121449. https://doi.org/10.1016/j.ijheatmasstransfer.2021.121449.

[22] B. Abramzon, S.S. Sazhin, Convective vaporization of fuel droplets with thermal radiation absorption, Fuel 85 (1) (2006) 32-46. https://doi.org/10.1016/j.fuel.2005.02.027.

[23] S.S. Sazhin, T. Kristyadi, W.A. Abdelghaffar, S. Begg, M.R. Heikal, S.V. Mikhalovsky, S.T. Meikle, O. Al-Hanbali, Approximate analysis of thermal radiation absorption in fuel droplets, ASME J Heat Transfer 129 (2007) 1246-1255.

[24] H.C. van de Hulst, Light Scattering by Small Particles. New York, John Wiley, 1957.

[25] F.P. Incropera, D.P. DeWitt, Fundamentals of Heat and Mass Transfer. New York: John Wiley & Sons, 1996.

[26] V.S. Zubkov, G.E. Cossali, S. Tonini, O. Rybdylova, C. Crua, M. Heikal, S.S. Sazhin, Mathematical modelling of heating and evaporation of a spheroidal droplet, Int. J. Heat Mass Transfer 108 (2017) 2181-2190. DOI: http://dx.doi.org/10.1016/j.ijheatmasstransfer.2016.12.074

[27] G.V. Kuznetsov, P.A. Strizhak, R.S. Volkov, O. V. Vysokomornaya, Integral characteristics of water droplet evaporation in high temperature combustion products of typical flammable liquids using SP and IPI methods, Int. J. Therm. Sci. 108 (2016) 218-234. https://doi.org/10.1016/j.ijthermalsci.2016.05.019

[28] D. Antonov, O. Vysokomornaya, M. Piskunov, N. Shlegel, Analysis of statistical data on drop collisions in an aerosol flow during experiments, EPJ Web Conf. 196 (2019) 00013. https://doi.org/10.1051/epjconf/201919600013.

Figure Captions

Figure 1 (a) A schematic presentation of the set-up used in the experiments with ethanol and propane/butane mixture burners. (b) Ambient temperature distribution inside and in the vicinity of the ethanol (filled squares) and propane/butane mixture (filled circles) burners.

Figure 2 Video frames showing puffing of an emulsion droplet (a) and micro-explosion via puffing of a two-component droplet (b) placed in ethanol flame. Volume fractions of rapeseed oil and water in droplets were 90% and 10%, respectively. Droplets were located inside the flame at h = 1.5 ± 0.1 cm (see Figure 1b), where gas temperature was 1,120 K, and their initial radii were $R_{d0} = 0.5 \pm 0.025$ mm.

Figure 3 The times to puffing/micro-explosion versus initial radii of two-component droplets introduced into the ethanol (filled squares) and propane/butane mixture (filled circles) flames at h = 1.5 ± 0.1 cm (see Figure 1b). Volume fractions of rapeseed oil and water in droplets were 90% and 10%, respectively. Gas temperatures for ethanol and propane/butane mixture flames in this location were 1,120 K and 1,400 K, respectively.

Figure 4 The times to puffing/micro-explosion in droplets versus ambient gas temperature (a) and distance h (b) in an ethanol flame. Filled circles refer to two-component droplets; filled stars refer to emulsion droplets. In all cases, droplet initial radii were $R_{d0} = 0.78 \pm 0.025$ mm; volume fractions of rapeseed oil and water in droplets were 90% and 10%, respectively.

Figure 5 Ratios of the total surface mean areas of droplets after (S_c) and before (S_0) their disintegration versus ambient gas temperature. Droplet initial parameters are the same as in Figure 4. Filled circles refer to two-component

droplets; filled stars refer to emulsion droplets.

Figure 6 The plots of the numbers of child droplets produced during puffing (1) and micro-explosion (2) versus child droplet radii.

Figure 7 The times to puffing/micro-explosion of two-component rapeseed oil/water droplets introduced into the ethanol (a) and propane/butane mixture (b) flames versus droplet radii. The volume fractions of rapeseed oil and water were 90% and 10% respectively. Curves 1 show the experimental data; curves 2 show the predictions of the model when the effects of radiation and support were ignored; curves 3 show the predictions of the model when the effects of the support were taken into account, but the effects of radiation were ignored; curves 4 show the predictions of the model when the effects of radiation and support were taken into account.

Figure 8 The times to puffing/micro-explosion of the same droplets as in Figure 7 introduced into the ethanol (a) and propane/butane mixture (b) flames versus droplet radii. Curves 1 show the times to puffing/micro-explosion assuming that these processes start when the temperature at the water/rapeseed oil interface is equal to water boiling temperature $T_w = T_B$. Curves 2 show the same times but assuming that these processes start when the temperature at the water/rapeseed oil interface is equal to water nucleation temperature $T_w = T_N$.

Figure A A typical example of the image processing using Matlab to infer the number and radii of child droplets.

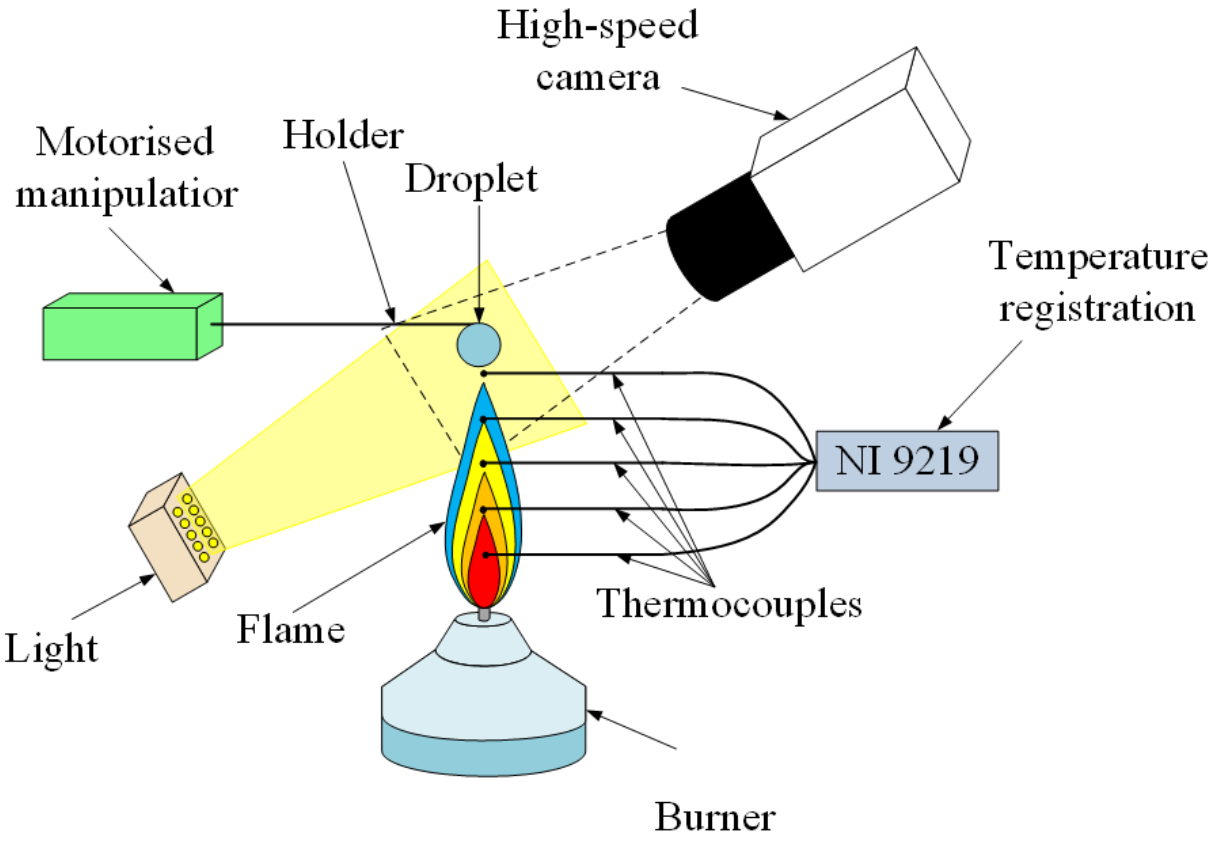
High-speed
camera
Motorised
manipulatior
Holder
Droplet
Temperature
registration
NI 9219
Thermocouples
Light
Flame
Burner

(a)

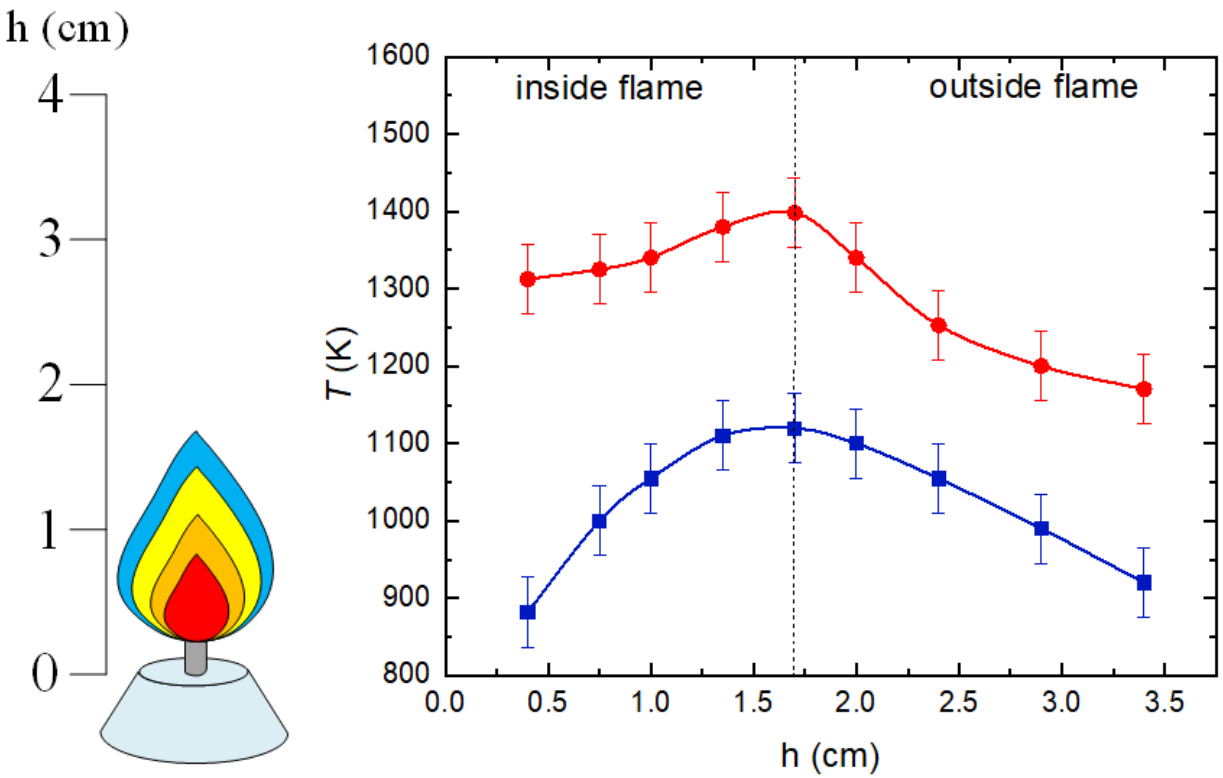
h (cm)
4
3
2
1
0
inside flame
outside flame
T (K)
1600
1500
1400
1300
1200
1100
1000
900
800
0.0
0.5
1.0
1.5
2.0
2.5
3.0
3.5
h (cm)

(b)

Fig. 1

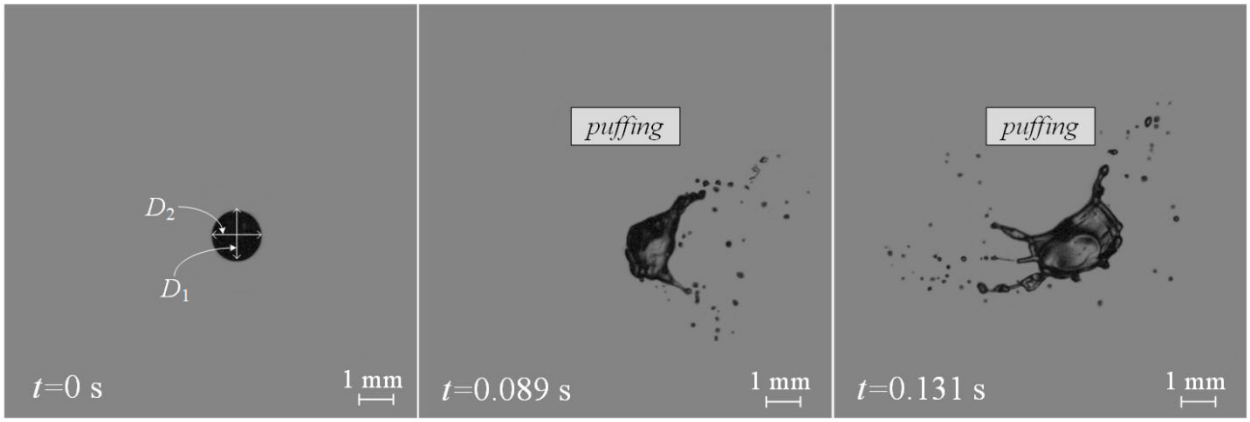
D_2
D_1
t=0 s
1 mm
puffing
t=0.089 s
1 mm
puffing
t=0.131 s
1 mm

(a)

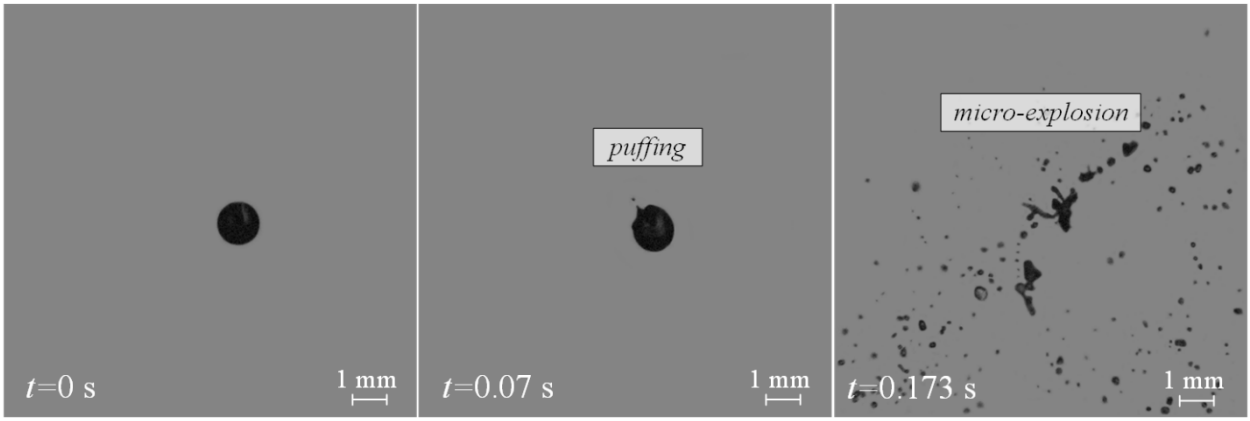
t=0 s
1 mm
puffing
t=0.07 s
1 mm
micro-explosion
t=0.173 s
1 mm

(b)

Fig. 2

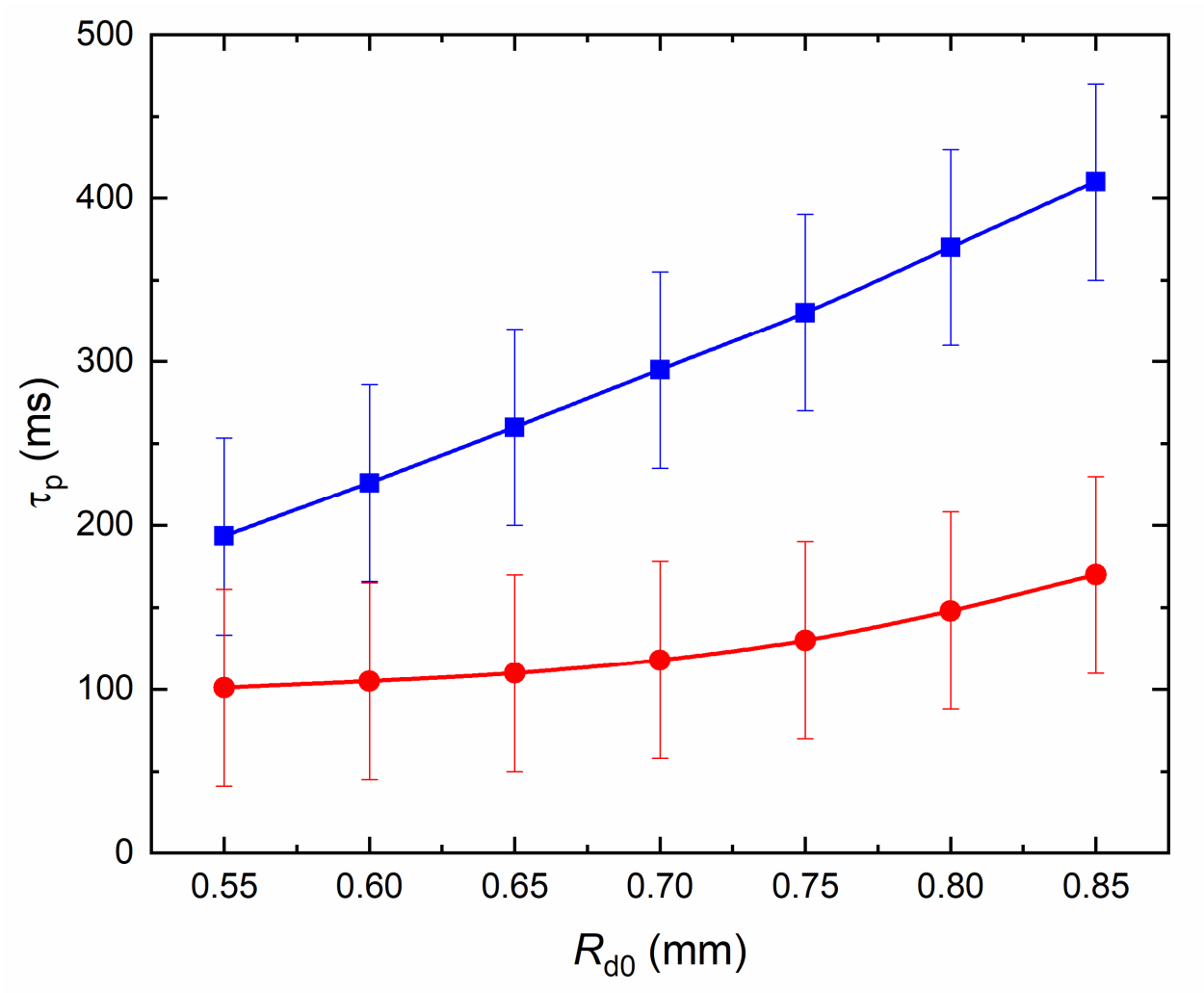

Fig. 3

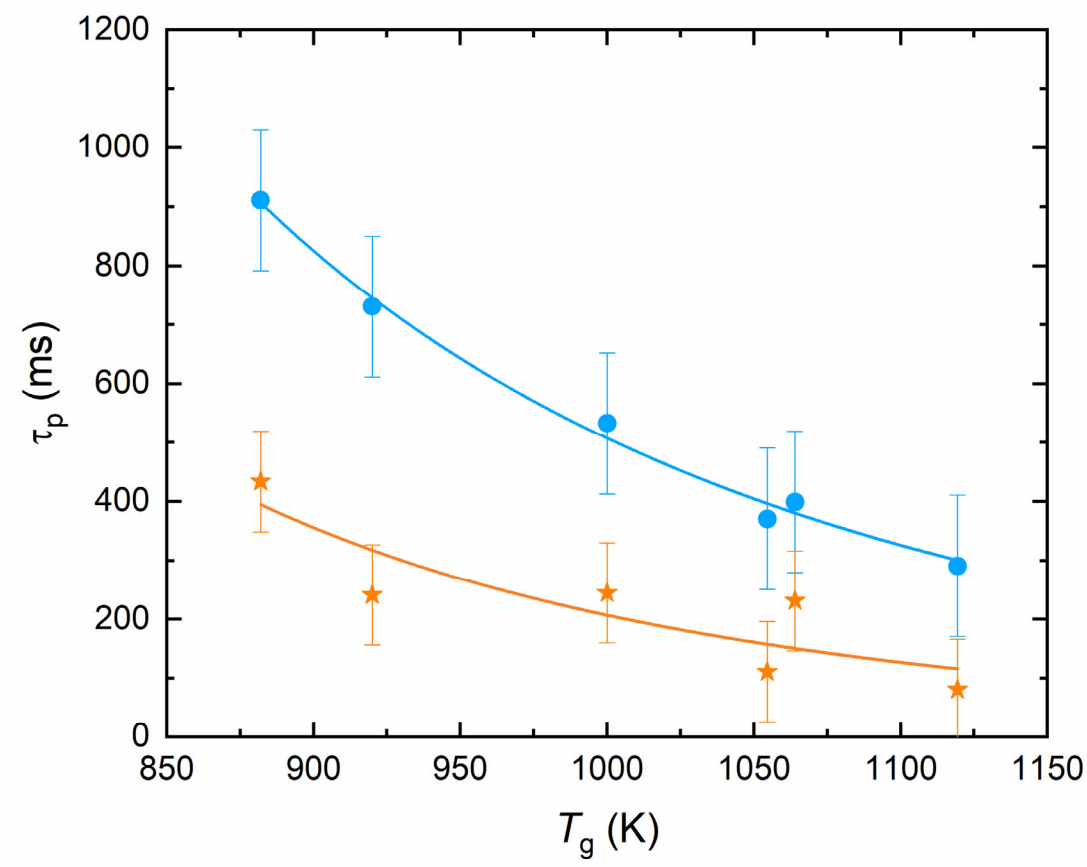
1200
1000
800
600
400
200
0
τ_p (ms)
850
900
950
1000
1050
1100
1150
T_g (K)

(a)

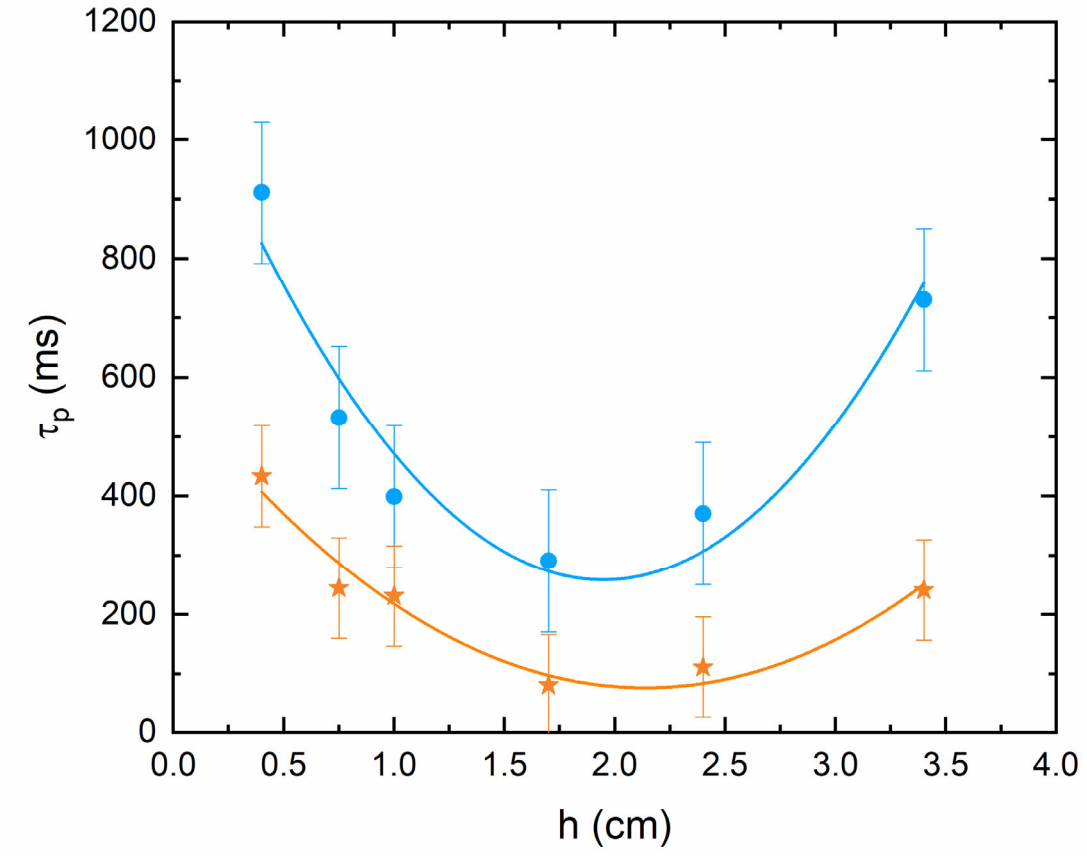
1200
1000
800
600
400
200
0
τ_p (ms)
0.0
0.5
1.0
1.5
2.0
2.5
3.0
3.5
4.0
h (cm)

(b)

Fig. 4

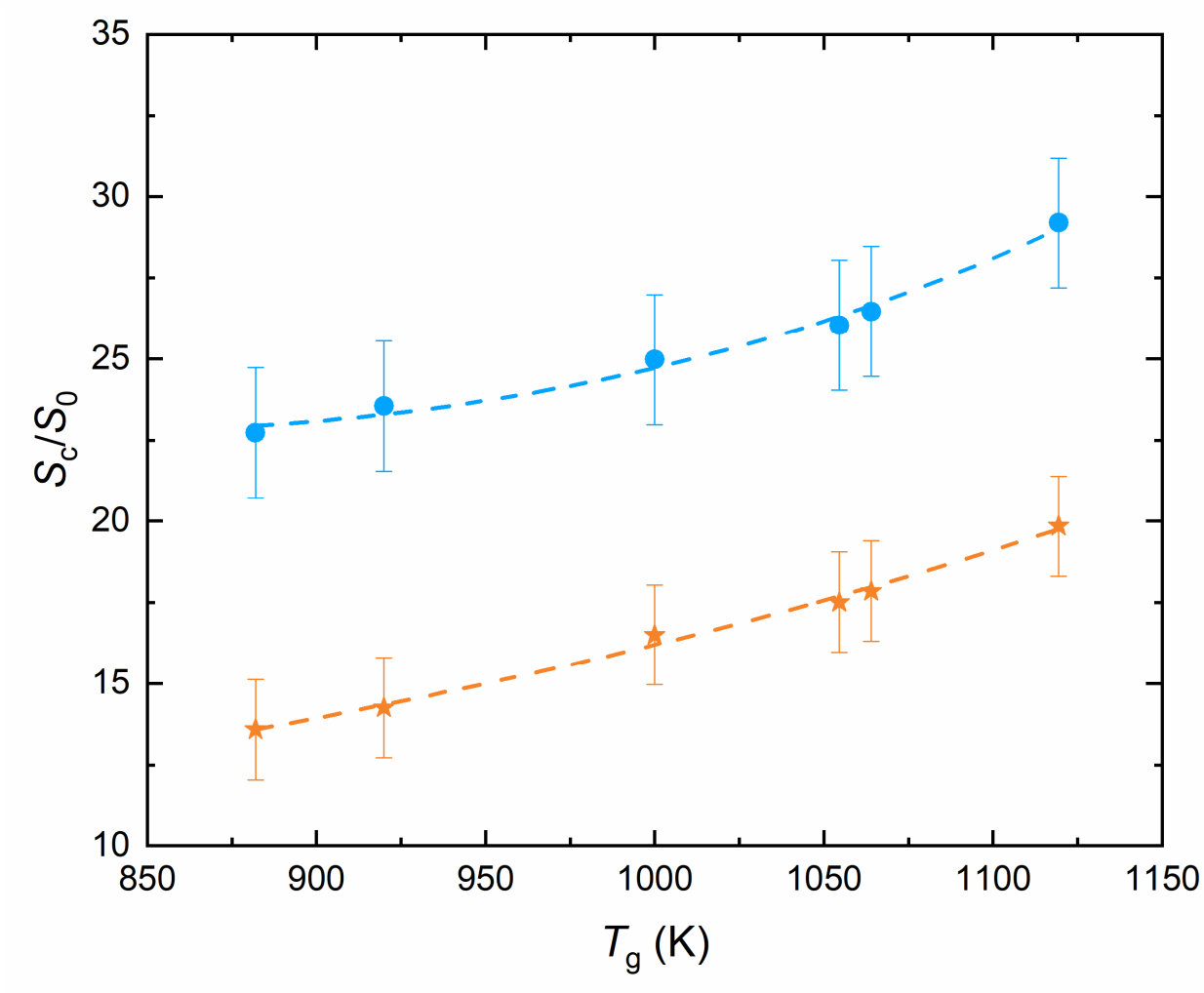

Fig. 5

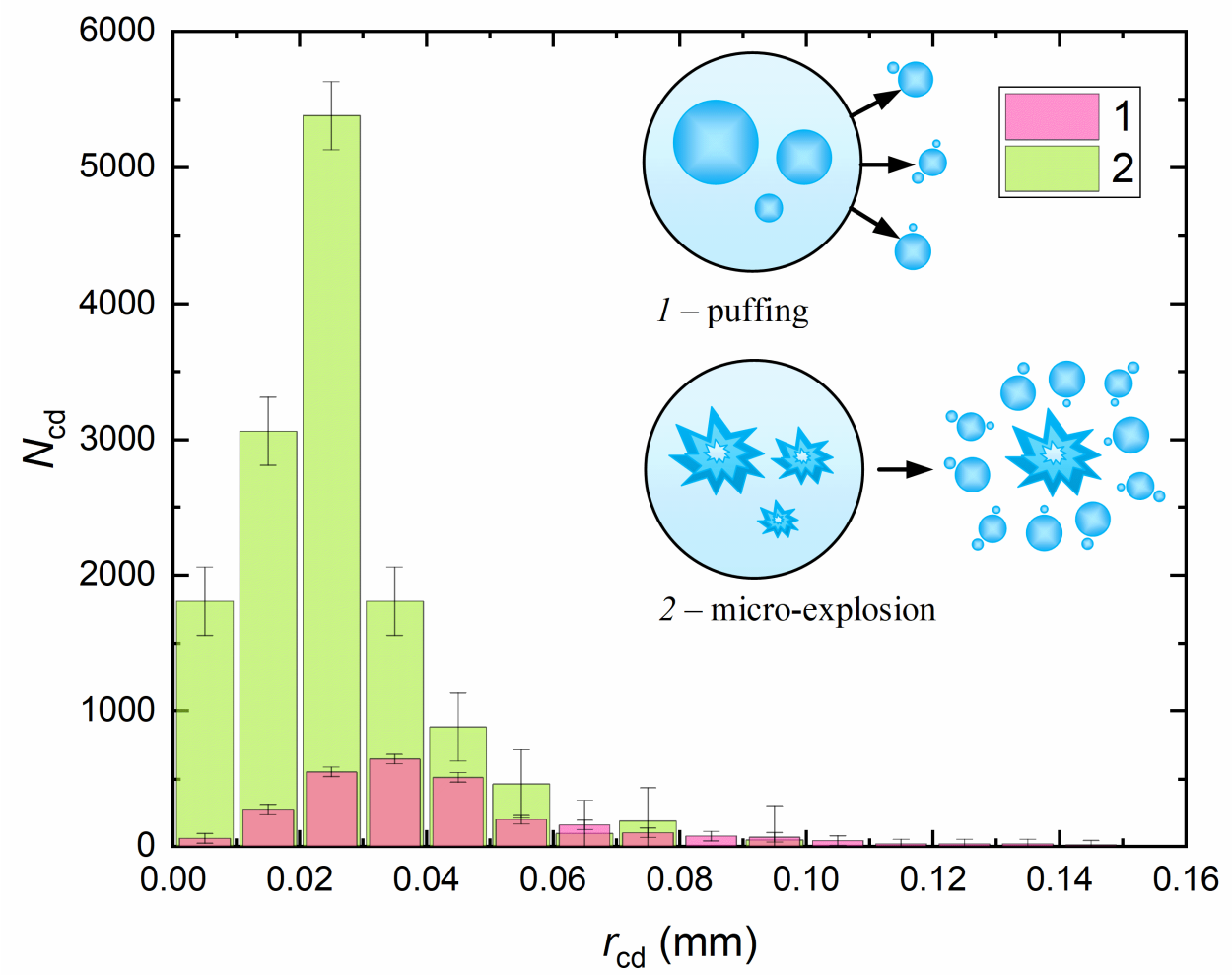
6000
5000
4000
3000
2000
1000
0
N_{cd}
0.00
0.02
0.04
0.06
0.08
0.10
0.12
0.14
0.16
r_{cd} (mm)
1
2
1 – puffing
2 – micro-explosion

Fig. 6

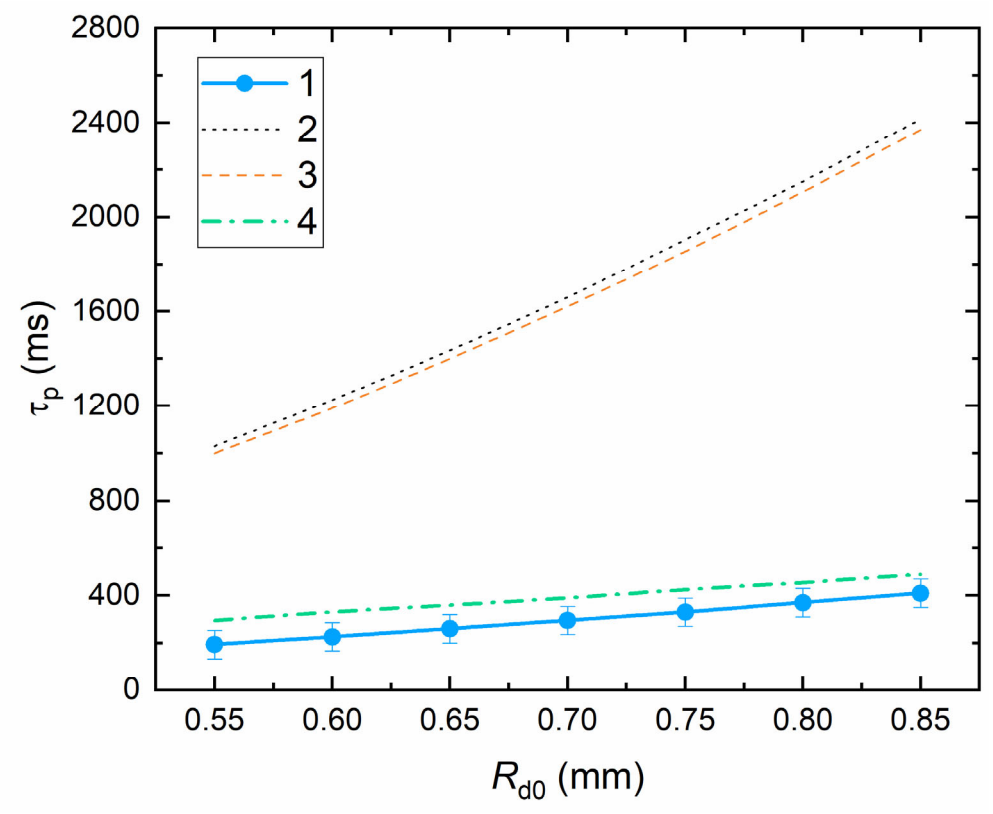
2800
2400
2000
1600
1200
800
400
0
τ_p (ms)
1
2
3
4
0.55
0.60
0.65
0.70
0.75
0.80
0.85
R_{d0} (mm)

(a)

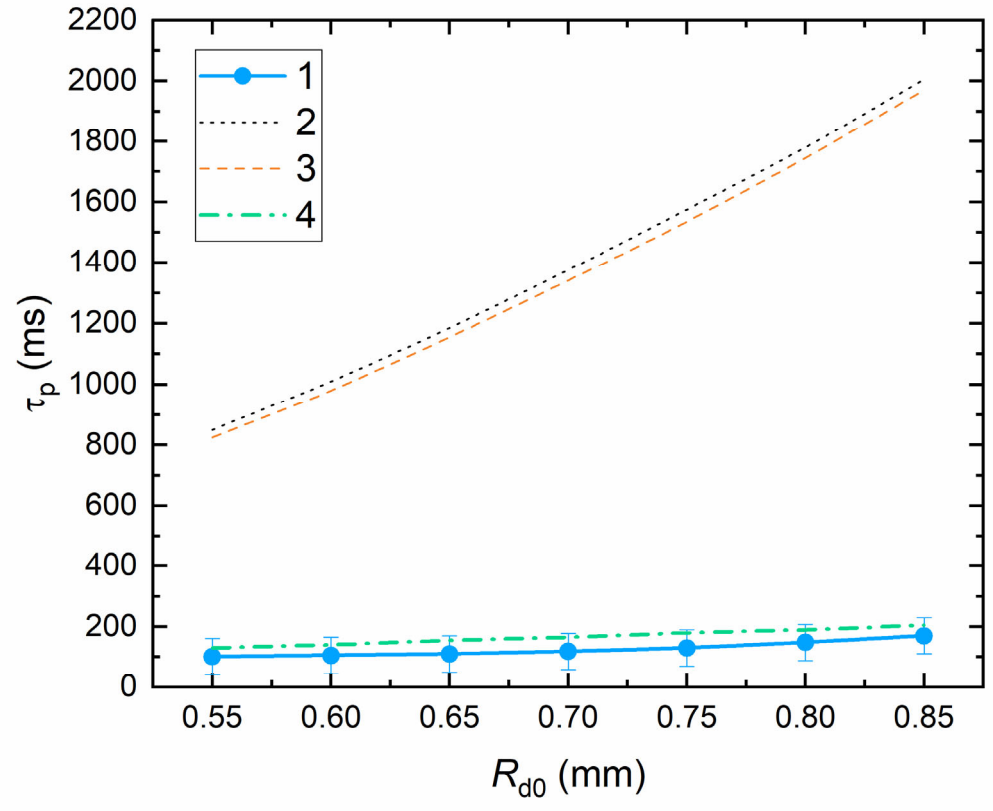
2200
2000
1800
1600
1400
1200
1000
800
600
400
200
0
τ_p (ms)
1
2
3
4
0.55
0.60
0.65
0.70
0.75
0.80
0.85
R_{d0} (mm)

(b)

Fig. 7

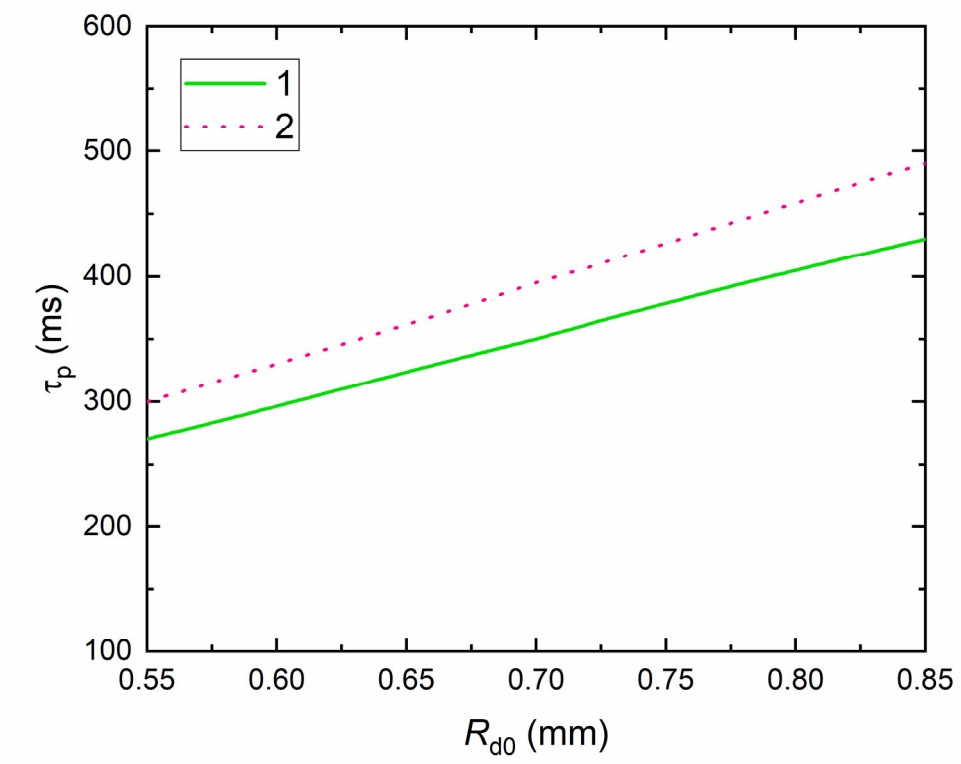
600
500
400
300
200
100
1
2
τp (ms)
0.55
0.60
0.65
0.70
0.75
0.80
0.85
Rd0 (mm)

(a)

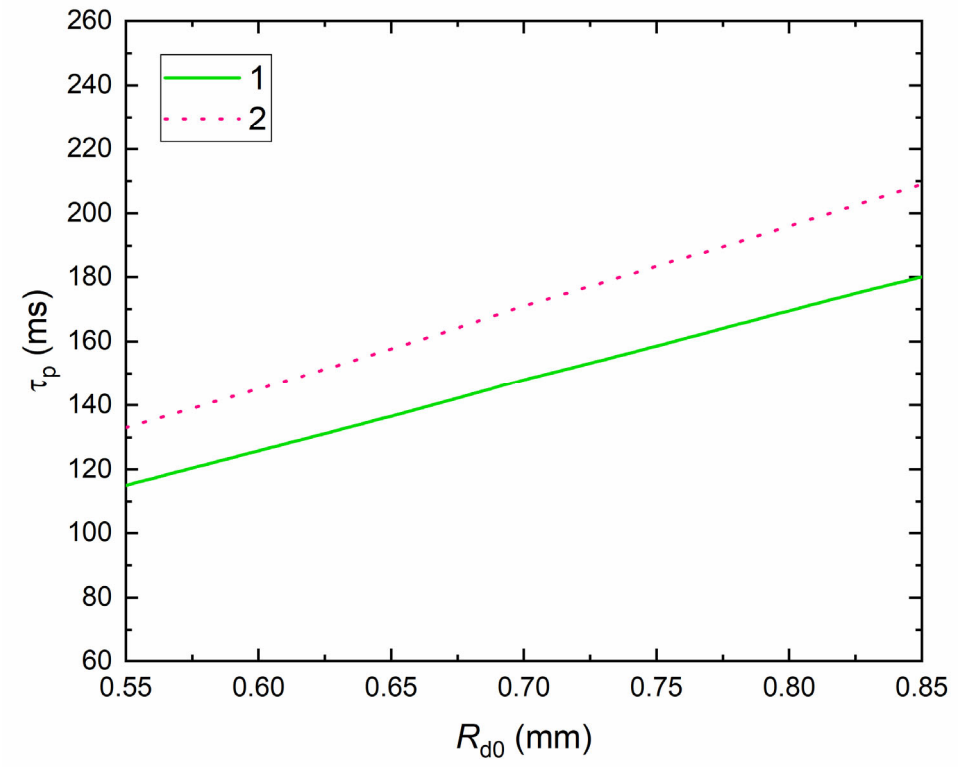
260
240
220
200
180
160
140
120
100
80
60
1
2
τp (ms)
0.55
0.60
0.65
0.70
0.75
0.80
0.85
Rd0 (mm)

(b)

Fig. 8

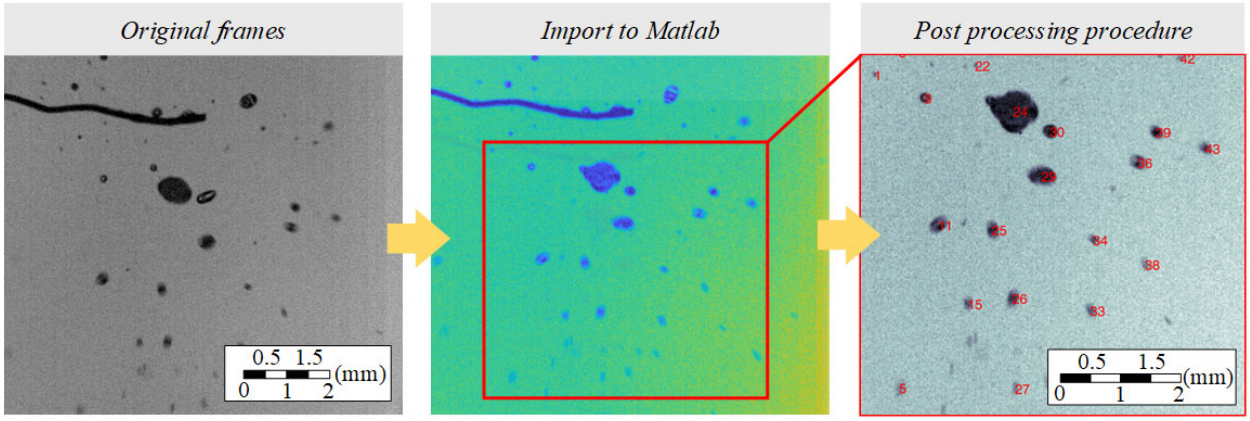
Original frames
Import to Matlab
Post processing procedure
0.5 1.5
0 1 2 (mm)
0.5 1.5
0 1 2 (mm)

Fig. A